OPTIMISATION OF THE PARAMETERS IN COMPLEX-PADÉ FOURIER FINITE-DIFFERENCE MIGRATION

M. Salcedo, A. Novais, J. Schleicher, and H. B. Santos

email: *amelia@ime.unicamp.br, js@ime.unicamp.br*

keywords: *Depth migration, Fourier finite-difference, complex Padé approximation, parameter optimisation, steep dips*

ABSTRACT

Fourier finite-difference migration (FFD) is an hybrid method that tries to improve on the inherent dip-limitation of one-way wave-equation based migration. One shortcoming of the conventional real Padé approximation used in the operator is the incorrect treatment of evanescent modes. This limitation can be strongly improved with the complex Padé approximation of the square-root. The dip limitation of the FFD operator depends on the variation of the velocity field and has been treated in real-Padé FFD by optimisation of the velocity-dependent parameter σ. In this work, we extend this parameter optimisation to complex-Padé FFD. We discuss the achieved quality of the approximate dispersion relation for different σ functions under consideration of the number of terms in the Padé approximation and the branch-cut rotation angle. The highest dip angles can actually be reached with a one-term Padé expansion. The associated σ function that leads to the highest imageable dip angles can be well-adjusted by a 4th-order polynomial. The implementation is validated on the Marmousi model dataset.

INTRODUCTION

Fourier finite-difference (FFD) migration (Ristow and Rühl, 1994) was designed as a correction to split-step migration (Stoffa et al., 1990) to improve the migrated images of strongly-dipping reflectors in media with strong velocity variations. It is an improved approximation of the square-root operator involved in one-way wave-equation migration by means of a Padé series, adding a finite-difference correction term to the split-step approximation. While one-way wave-equation methods have gone out of fashion with the advent of more powerful computers that allow for the standard use of two-way methods, such tools are still of interest for modern methods like Marchenko imaging (Wapenaar et al., 2014).

In the original work of Ristow and Rühl (1994), the authors used the real Padé series. This implies in a real approximation of the square root even for evanescent waves, where the dispersion relation should become complex. As a consequence, evanescent waves, which should propagate horizontally with damping in the vertical direction, are propagated into the medium without amplitude decay, causing acausal precursors to the wavefield. These, in turn, may lead to artifacts or even spurious reflectors in the migrated image.

For this reason, Amazonas et al. (2007) replaced the real Padé approximation by the complex one of Milinazzo et al. (1997). They showed that in this way, the evanescent waves are better treated. While still presenting nonzero real parts of the vertical wave-vector components, i.e., still propagating into the medium, they are now damped vertically. In this way, the migrated images contain less artifacts, becoming of comparable quality as the images obtained with the much more expensive FFD plus interpolation of Biondi (2002).

Ristow and Rühl (1994) demonstrate that the theoretically derived expression for the parameter σ as a function of the ratio between reference and model velocities does not provide the best steep-angle images

in real-Padé FFD migration. They showed for a single term of the Padé series that an optimised function σ further increases the imageable dips. Amazonas et al. (2007) did not carry out such an optimisation for complex-Padé FFD migration (CPFFD). They only indicated that a heuristically chosen function improved the dip behavior of CPFFD for a three-term Padé approximation.

In this work, we discuss the behavior of CPFFD migration in dependence on the selected function for σ, as well as on the branch-cut rotation angle and the number of terms used in the Padé approximation. We exhibit an optimised σ function for the best possible choices of the rotation angle and show that for certain ratios between the reference and model velocities, the best dip-angle behavior is achieved with a single Padé term, while for other values of that ration, two terms are advantageous. We validate the observations on a synthetic data set from the Marmousi model.

DOWNWARD-CONTINUATION MIGRATION

The one-way acoustic wave equation for downward continuation the $k_x - \omega$ domain reads (Claerbout, 1985)

$$\frac{\partial P(k_x, z, \omega)}{\partial z} = -\frac{\imath\omega}{v}\sqrt{1 - \left(\frac{vk_x}{\omega}\right)^2}\, P(k_x, z, \omega)\ . \tag{1}$$

In other words, the vertical wavenumber k_z can be expressed by the following dispersion relation, which is often called the Single Square Root (SSR) equation,

$$k_z = SSR(k_x, \omega) = -\sqrt{\frac{\omega^2}{v^2} - k_x^2} = -\frac{\omega}{v}\sqrt{1 - \left(\frac{vk_x}{\omega}\right)^2}\ . \tag{2}$$

For a laterally varying medium velocity v, equation (1) is a pseudo-differential equation, where k_x represents the symbol of the horizontal derivative. Therefore, to numerically evaluate the operator, the square-root has to be approximated. This leads to dip-limited migration methods (Claerbout, 1985).

Phase-shift migration

When propagation velocity is assumed to be a function only of depth, wavefield can be downward-continued efficiently in the frequency-wavenumber $\omega - k$ domain by simple multiplication with the SSR downward-continuation operator,

$$P(k_x, z + \Delta z, \omega) = P(k_x, z = 0, \omega) e^{-\frac{\imath\omega}{v}\sqrt{1 - \left(\frac{vk_x}{\omega}\right)}\Delta z}\ . \tag{3}$$

The downward-continuation operator expressed in equation (3) describes a dip-dependent k_x/ω phase shift of the wavefield; thus, it often is called the phase-shift operator (Gazdag, 1978). When the medium's velocity is not strictly a function of depth, application of equation (3) with some average or reference velocity can still approximately work if the lateral variations are very small. In order to handle slightly larger lateral velocity variations, Gazdag and Sguazzero (1984) introduced the phase-shift plus interpolation (PSPI) method. Instead of only one velocity at each depth step, it uses several reference velocities to propagate several reference wavefields. The approximate final wavefield is obtained by linearly interpolating the reference wavefields based on the relationship of the local velocity to the reference velocities.

Split-step migration

A more elegant approach to the lateral velocity variations was provided by split-step migration (Stoffa et al., 1990). They noted that when propagating a reference wavefield with a reference velocity, even vertical propagation is incorrect. Therefore, they corrected the SSR operator in the space domain for this error, i.e.,

$$k_z = SSR(k_x, \omega) \approx \left(\sqrt{\frac{\omega^2}{v_{ref}^2} - k_x}\right) + \left(\frac{\omega}{v(x,z)} - \frac{\omega}{v_{ref}}\right) = PS + SS\ , \tag{4}$$

where the correction term SS is the difference between the true square root SSR and its phase-shift approximation PS for $k_x = 0$. For migration, the operator implementing the PS term in expression (4) is applied in the ω-k domain according to equation (3), whereas the SS term represents a spatially varying time shift that easily can be applied in the ω-x domain.

Fourier finite-difference migration

To find a better approximation for the difference between the true and reference square roots Ristow and Rühl (1994) approximated both of them by means of a first-order continued-fraction expression,

$$\sqrt{1-Z} \approx 1 - \frac{Z}{2 - \frac{Z}{2}} \,, \tag{5}$$

where $Z = (vk_x/\omega)^2$. Actually, this approximation can also be interpreted as the first term of a Padé series,

$$\sqrt{1-Z} \approx 1 - \sum_{n=1}^{N} \frac{a_n Z}{1 - b_n Z} \,, \tag{6}$$

with the Padé coefficients (Bamberger et al., 1988)

$$a_n = \frac{2}{2N+1} \sin^2\left(\frac{n\pi}{2N+1}\right) \qquad \text{and} \qquad b_n = \cos^2 \frac{n\pi}{2N+1} \,. \tag{7}$$

By expanding the continued-fraction terms (5) of both square roots into Taylor series, joining them, and regrouping the terms back into the form of a continued fraction, Ristow and Rühl (1994) derived the FFD approximation

$$k_z = SSR(k_x, \omega) \approx PS + SS + p(1-p)\frac{a_1 Z}{1 - b_1 \sigma(p) Z} \,, \tag{8}$$

where $p = v(x,z)/v_{ref}$ and where a_1 and b_1 are the Padé coefficients of equation (7) with $n = N = 1$, i.e., $a_1 = 1/2$ and $b_1 = 1/4$. Moreover, $\sigma(p) = 1 + p + p^2$. The FFD correction term is then applied in the ω-x domain by means of a finite-difference operator very similar to the one used in FD migration. As shown by Ristow and Rühl (1994), conventional FFD schemes become instable if $p > 1$. Biondi (2002) was able to overcome that problem by an intelligent symmetrical decomposition of the operator.

Complex-Padé Fourier finite-difference migration

The real-valued coefficients given in equation (7), while useful for certain problems, result in a square-root approximation which maps the real axis onto itself. However, if $Z < -1$, the left side is a purely imaginary number but the right side remains a real-valued quantity. In other words the approximation breaks down. In the context of wave propagation, this leads to inappropriate treatment of evanescent modes and poor approximation for high propagation angles. This difficulty can be overcome by using complex coefficients. Milinazzo et al. (1997) propose a complex representation of the Padé expansion in equation (6). They chose the branch cut to lie in the negative half-plane, rotated from the negative axis by an angle α. Figure 1 shows the rotation of the branch cut in the complex plane.

Using the complex expressions of Milinazzo et al. (1997), Amazonas et al. (2007) follow the real-valued derivation of Ristow and Rühl (1994) to derive the complex-Padé FFD algorithm. Their final expression is

$$k_z = SSR(k_x, \omega) \approx PS + C_0 SS + p(1-p) \sum_{n=1}^{N} \frac{A_n Z}{1 - B_n \sigma(p) Z} \,, \tag{9}$$

where

$$A_n \equiv \frac{a_n e^{-\frac{\imath\alpha}{2}}}{\left[1 + b_n(e^{-\imath\alpha} - 1)\right]^2} \,, \qquad B_n \equiv \frac{b_n e^{-\imath\alpha}}{1 + b_n(e^{-\imath\alpha} - 1)} \,.$$

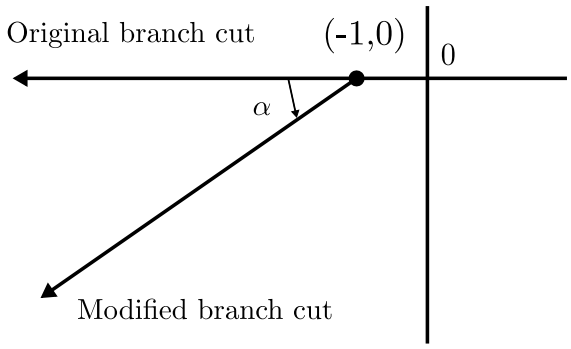

Figure 1: Branch cut rotation angle in the complex plane.

The number C_0 should, according to Milinazzo et al. (1997) and Amazonas et al. (2007), be correctly represented as

$$C_0 \equiv e^{\imath\frac{\alpha}{2}}\left[1+\sum_{n=1}^{N}\frac{a_n(e^{-\imath\alpha}-1)}{[1+b_n(e^{-\imath\alpha}-1)]}\right] .$$

However, this turns out to be a sophisticated approximation to one that gets the better the more terms N are used. Therefore, it can be directly replaced by $C_0 = 1$.

As numerically demonstrated by Amazonas et al. (2007), this complex-Padé approximation results in a better representation of the evanescent part of the mode spectrum than its real counterpart.

NUMERICAL EVALUATIONS

There are three important parameters to choose when implementing a CPFFD migration. These are the branch-cut rotation angle α, the number N of terms in the Padé series, and the function $\sigma(p)$. Below we discuss the influence of these parameters on the dispersion relation.

Methodology

Amazonas et al. (2007) have provided a preliminary analysis of the branch-cut rotation angle. Figure 2 reproduces the approximation of the dispersion relation for a rather small value of $p = 0.5$ for three different rotation angles α of $5°$, $45°$ and $90°$, respectively. From this analysis, Amazonas et al. (2007) concluded that the best rotation angle was $45°$, and they recommended $\sigma = 1 + p^3$ over the theoretical function $\sigma = 1+p+p^2$ to reach higher dip angles. However, as we will se below, there are better functions σ, and for those, the choice of the rotation angle must be revisited.

Error analysis

To find the optimal choice for the CPFFD parameters, we follow the fairly simple idea of Ristow and Rühl (1994). Basically, we systematically study the relative error behavior of the dispersion relation for a series of values of σ for each chosen but fixed value of p. Since the tolerable positioning error of migration is often associated with one percent error of the dispersion relation (Ristow and Rühl, 1994), we look for a combination of parameters that will maximise the dip angle where this error of one percent occurs. In this way, we determine the quality of a certain approximation by means of the intersection of the relative error function with the one percent error line.

The relative error is defined by

$$E(X) = E(\sin\theta) \quad = \quad 100\,\frac{\varepsilon}{\sqrt{1-\left(\frac{k_x}{k}\right)^2}}\,, \tag{10}$$

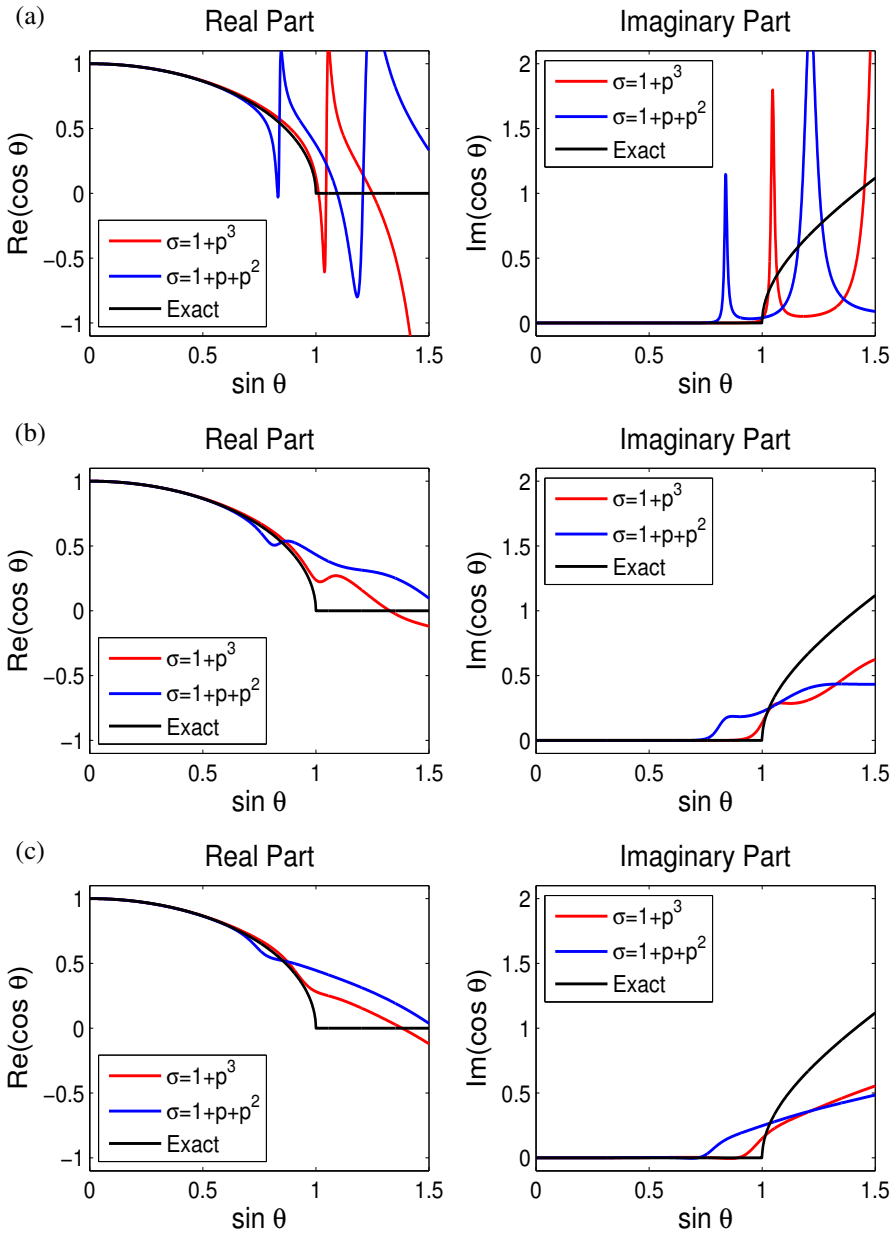

Figure 2: Complex Padé approximations to the dispersion relation with different branch-cut rotation angles. (a) $\alpha = 5°$; (b) $\alpha = 45°$; (c) $\alpha = 90°$.

where ε is the absolute error, i.e., the difference between the square root and its approximation. The maximum dip angle of a migration operator is then defined as that angle that gives a relative error of one percent, $E(\sin\theta) = 0.01$. Figure 3 shows such an analysis for the case of $\sigma = 1 + p^3$ in a 3-term approximation for $\alpha = 90°$. For this case, we obtain $\sin\theta = 0.6285$, which corresponds to a maximum dip angle of $\theta = 38.94°$.

Defining the parameters of the Padé expansion

We decided to evaluate the number of terms in the Padé expansion, that means, to check if $N = 3$ terms is really the best option to approximate the downward-continuation operator. For this analysis, we determine

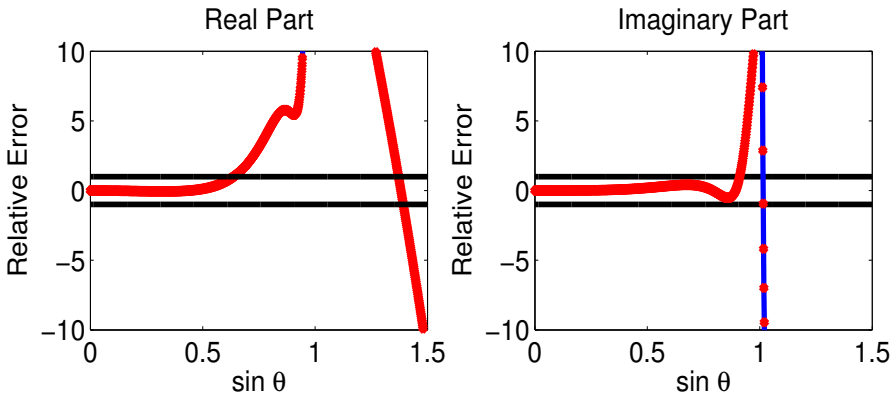

Figure 3: Relative error as a function of propagation angle.

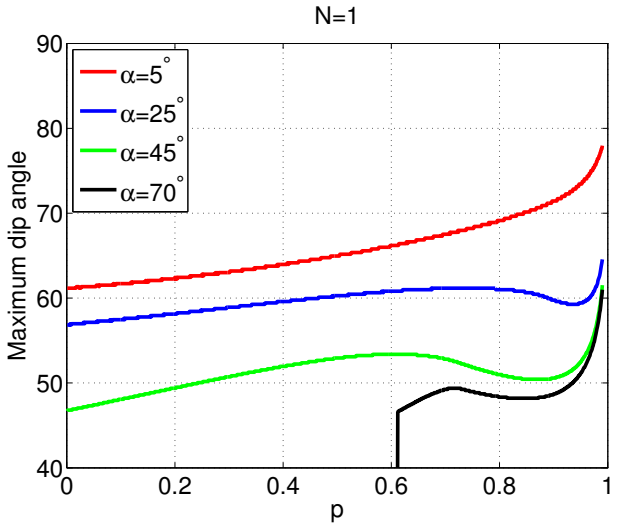

Figure 4: Maximum dip angle with $N = 1$ for best possible values of σ and different values of α.

for each value of p the value of σ that maximises the dip angle θ in dependence on the number N of terms used and on the rotation angle α. Figure 4 plots the so-obtained maximum dip angle for $N = 1$ for four different rotation angles. Note that each of the curves in this figure was determined with the specific function $\sigma(p)$ which maximises the dip for that rotation angle. We can immediately see that the maximum dip angle decreases with increasing rotation angle, indicating that $45°$ is probably not the best choice for the rotation angle for $N = 1$ as concluded for $N = 3$ by Amazonas et al. (2007). The variation for small angles close to $5°$ are rather small. Since a too small angle reintroduces propagating evanescent waves, we believe that $5°$ is the best possible choice for $N = 1$.

Figure 5 shows the same analysis for with $N = 2$ and 3 terms in the Padé expansion, respectively. Now we can conclude that for rotation angles higher than $45°$ we get weak dip angles, even with the optimal values of σ. For $N = 2$, our best result is obtained with $\alpha = 25°$ but we can see a weird "hole" in the middle, where the maximum dip angle suddenly decreases. Further tests with other angles between $25°$ and $29°$ (see Figure 6) showed that the first angle where this "hole" disappears, is $27°$, which thus is the optimal value of α for $N = 2$.

In the second part of Figure 5 we include a comparison to the dip angles reached by the heuristic function $\sigma = 1 + p^3$ of Amazonas et al. (2007). We see that there are still better values of σ than those, which allow to reach even higher dip angles. The choice of the rotation angles is less critical for $N = 3$.

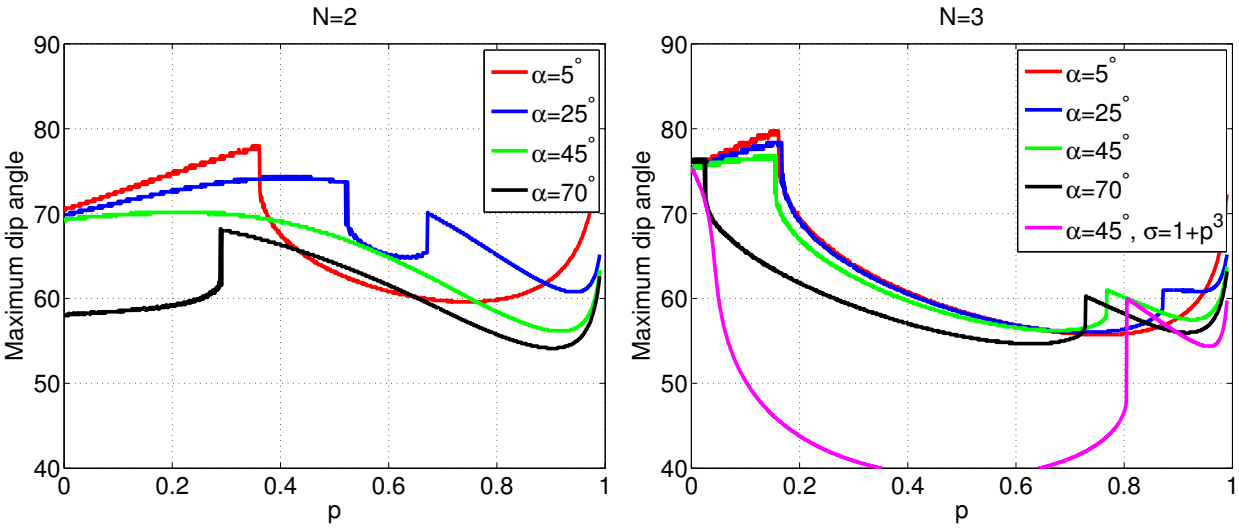

Figure 5: Maximum dip angle with $N = 2$ and $N = 3$.

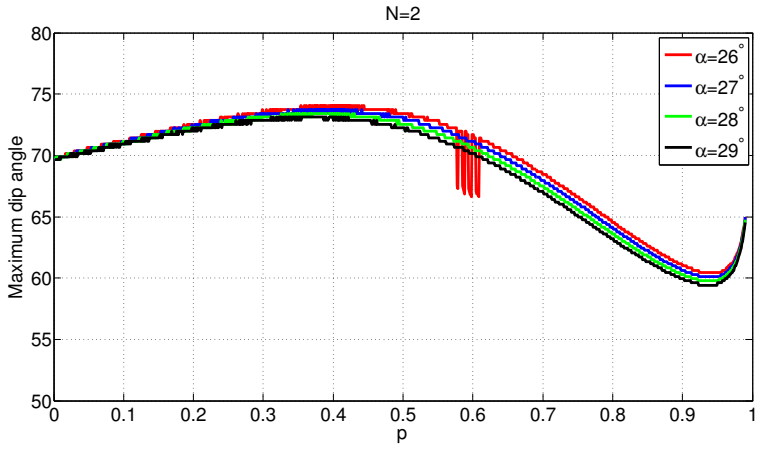

Figure 6: Defining the optimal value of α to be used with 2 terms.

All values between 5° and 45° lead to approximately the same dip-angle behavior, except for p values between 0.8 and 1. We already recognise from these figures that except for a small range of not very realistic values of p between 0.18 and 0.35, the CPFFD approximation reaches a higher dip angle with one or two terms than with three. That is actually good news because less terms in the Padé expansion mean lower computational cost.

For a corroboration of these findings, we now look at the comparison of the maximum dip angle as a function of N for fixed rotation angles. Figure 7 shows the maximum dip angle for $\alpha = 5^\circ$ for one and two Padé terms. We recognise that while two terms attain higher dip angles for p values below 0.45, the one-term approximation is actually better for higher p. Since that range of p is the more important one, this figure suggests that working with a single Padé term might actually produce the best migrated images. For higher rotation angles, the 1-term approximation reaches only lower angles, while the 2-term approximation does not change significantly (see Figure 8). Therefore, the highest dip angles can actually be imaged by the 1-term 5° approximation, at least in the p range of 0.45 to 1.0, reaching dip angles of more than 65°.

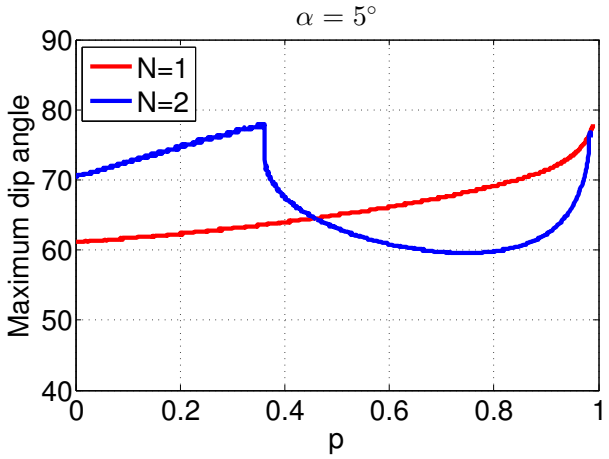

Figure 7: Maximum dip angle for $\alpha = 5°$.

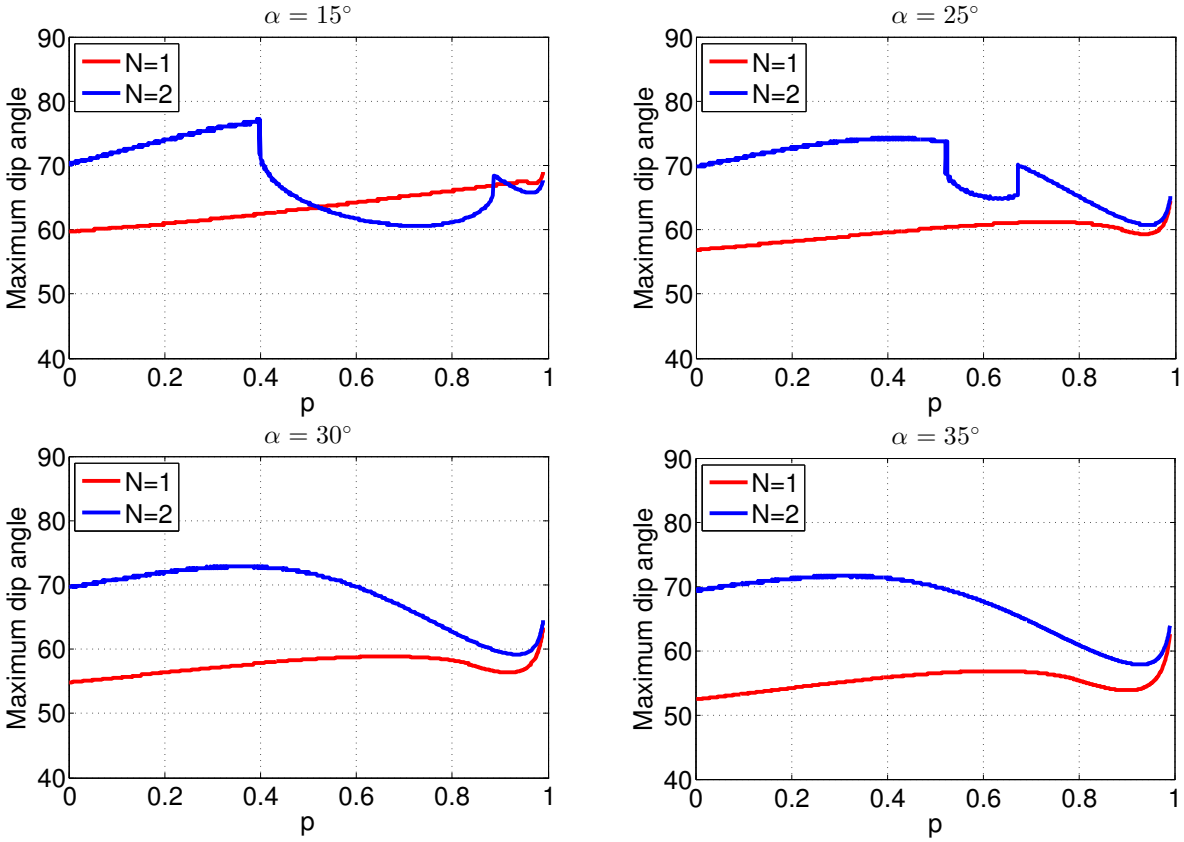

Figure 8: Maximum dip angle for $\alpha = 15°$, $\alpha = 25°$, $\alpha = 30°$, and $\alpha = 35°$.

Comparison to earlier results

The next analysis is to compare our results with the maximum dip angles attained by the approximations of Ristow and Rühl (1994) and Amazonas et al. (2007).

The left part of Figure 9 shows the maximum dip angles obtained with our optimised σ for a branch rotation angle of 5 degrees and only one term in the Padé expansion. Using the same parameters, we can see that the angles obtained using $\sigma = 1 + p + p^2$ give better results compared with the $\sigma = 1 + p^3$ used

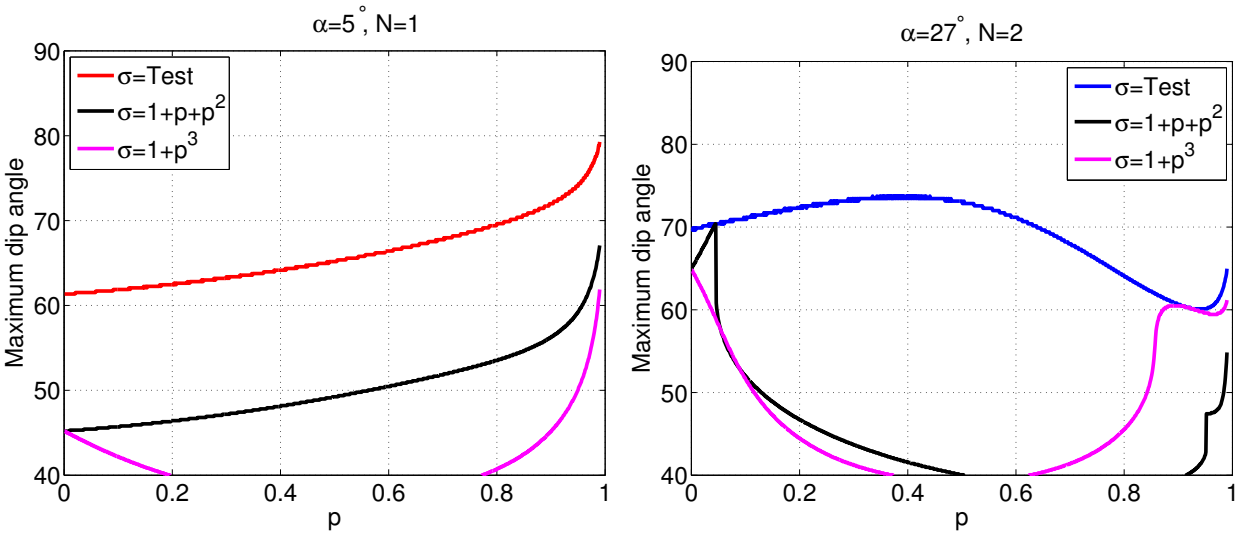

Figure 9: Optimised σ compared with the theoretical and heuristic σ functions. Left: $N = 1$, $\alpha = 5°$. Right: $N = 2$, $\alpha = 27°$.

by Amazonas et al. (2007), but none achieves the quality of the optimised σ.

The corresponding comparison for two Padé terms and a rotation angle of 27 degrees is depicted in the right part of Figure 9. In this case $\sigma = 1 + p^3$ achieves better dip angles than $\sigma = 1 + p + p^2$.

Comparing the parts of Figure 9, we also recognise that even for the best rotation angle of 27°, the 2-term approximation achieves higher dip angles only for p up to 0.7. For higher p values, the best 1-term approximation is still superior. This is confirmed in Figure 10, which compares the two results for the optimal σ functions with the best results from the literature for real (Ristow and Rühl, 1994) and complex-Padé (Amazonas et al., 2007) FFD.

The first observation is that the curve for $N = 3$, $\sigma = 1 + p^3$ and $\alpha = 45°$ cannot compete with the optimised σ results. Interestingly, the maximum dip angles obtained by the optimised σ curve of Ristow and Rühl (1994) for real-Padé FFD are virtually identical to those obtained for the $N = 1$, $\alpha = 5°$ case. This indicates that the brunch-cut rotation reduces the ability of FFD migration to image steep dips, but small rotation angles can still preserve the angles achieved in the real case. Note that even small rotation angles introduce damping of the evanescent modes and should be preferred over a completely real procedure.

Figure 10 also point out our second option to handle very strong lateral velocity variations, that is, using $\alpha = 27°$ and $N = 2$. These parameter values allow to reach maximum dip angles of more than 70° for p values below 0.7. The only problem of this parameter choice is the dip angle loss for p values closer to 1.0.

Optimised σ functions

The analysis for the optimal values of σ as a function of p can be summarised with the help of Figure 11. It depicts a color-coded image of the maximum dip angle as a function of p and σ. The curve of optimal values for σ for each value of p is clearly visible as only for a small range of σ values for each p, high maximum dip angles over 60 degree (red parts of the image) are reached. We recognise from this figure that for smaller values of p, a good choice of σ is rather important, while at values larger than 0.8, the region of high angles broadens, indicating that a perfect choice of the optimised σ is less crucial here. We notice that the range of optimum σ values is between 1.3 and 3.5.

The σ function

Our next goal is to see the σ function, its behavior and decide a good option to approximate or adjust the numerical values without the need for a table of values.

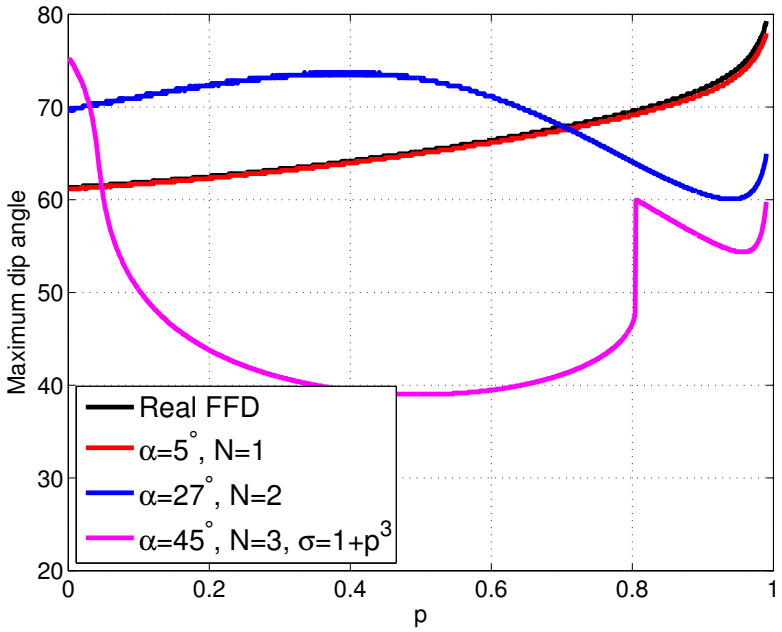

Figure 10: Angles obtained with the optimised σ compared with Real FFD and the results of Amazonas et al. (2007).

Figure 12 shows the optimal σ values versus all the possible values of p. The function is smooth, thus being easily adjustable with a polynomial function using least-squares. Figure 12 also depicts the so-adjusted 4th-order polynomial, given by $\sigma = 1.3255 + 0.54p + 4.1453p^2 - 6.5786p^3 + 4.2425p^4$. The adjusted polynomial presents good fit to the optimised values, with the only visible deviation in the region of $p > 0.8$, where perfect adjustment is not needed as explained above.

MIGRATION RESULTS

Marmousi model

We have used an implementation of the wide-angle complex FFD approximations of Amazonas et al. (2007) to perform prestack depth migration in 2D.

To evaluate the performance of the different parameterisations in a inhomogeneous medium, we compare their results in the true Marmousi velocity model (Versteeg, 1994), i.e., without any smoothing (Figure 13(a)). The imaging condition is the cross-correlation of the downward-continuation up going wavefield and down going wavefield from the source at zero time lag. The source wavelet was computed using a Ricker wavelet with 25-Hz peak frequency and a depth extrapolation depth size of 6 m.

Figure 13(b) and 13(c) compare the CPFFD migrations of the Marmousi dataset with the true Marmousi velocity model (Figure 13(a)) with the two parameter sets, the original parameters ($N = 3$, $\alpha = 45°$, $\sigma = 1 + p^3$) as presented by Amazonas et al. (2007) and our optimised parameters, respectively.

There are some subtle but visible differences between the images. Both of them are quite similar even in the central and deepest parts were the geology is fairly complex. While both images appear to resolve the faults, the steeper parts are better imaged in Figure 13(c) with the optimised parameter. On the other hand, there appear a few more artifacts in this figure, probably indicating that the damping of the evanescent modes is incomplete because of the small rotation angle.

However, it should not go unnoticed that the computation time required to produce the image depicted in Figure 13(b) is about twice the time we spent to produce the image shown in Figure 13(c). This confirms that our optimisation is about 50% faster with approximately the same results.

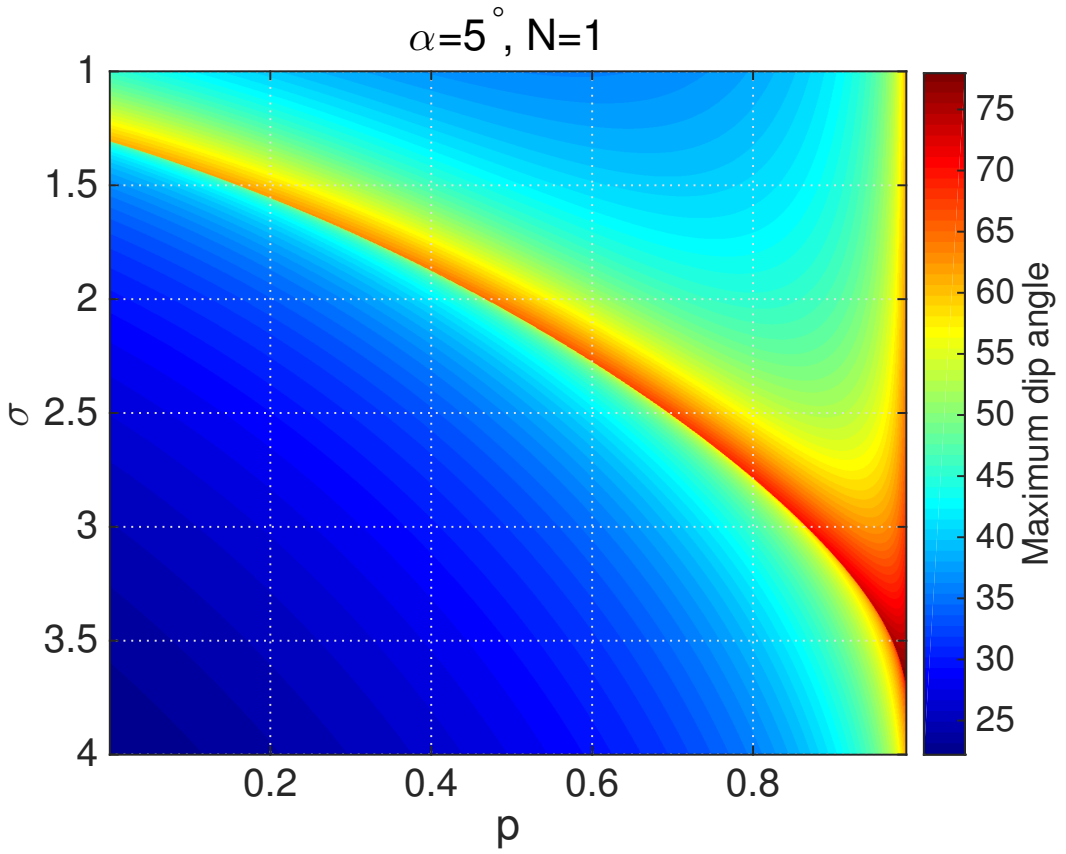

Figure 11: Maximum dip-angle values as a function of p and σ for the complex Padé approximation using $\alpha = 5°$ and $N = 1$.

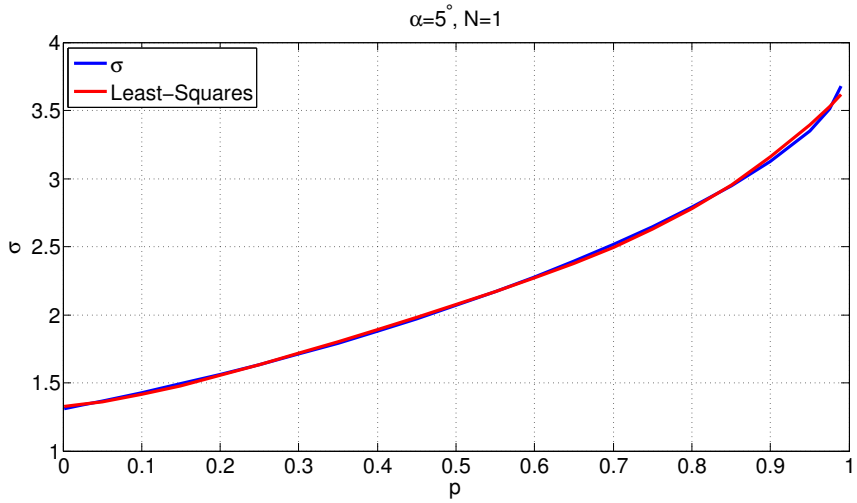

Figure 12: Optimised σ function versus least-squares.

CONCLUSIONS

In this work, we have investigated the optimisation of some parameters used in the complex-Padé FFD algorithm in order to extend the range of imageable reflector dips. Our original aim was to optimise σ in

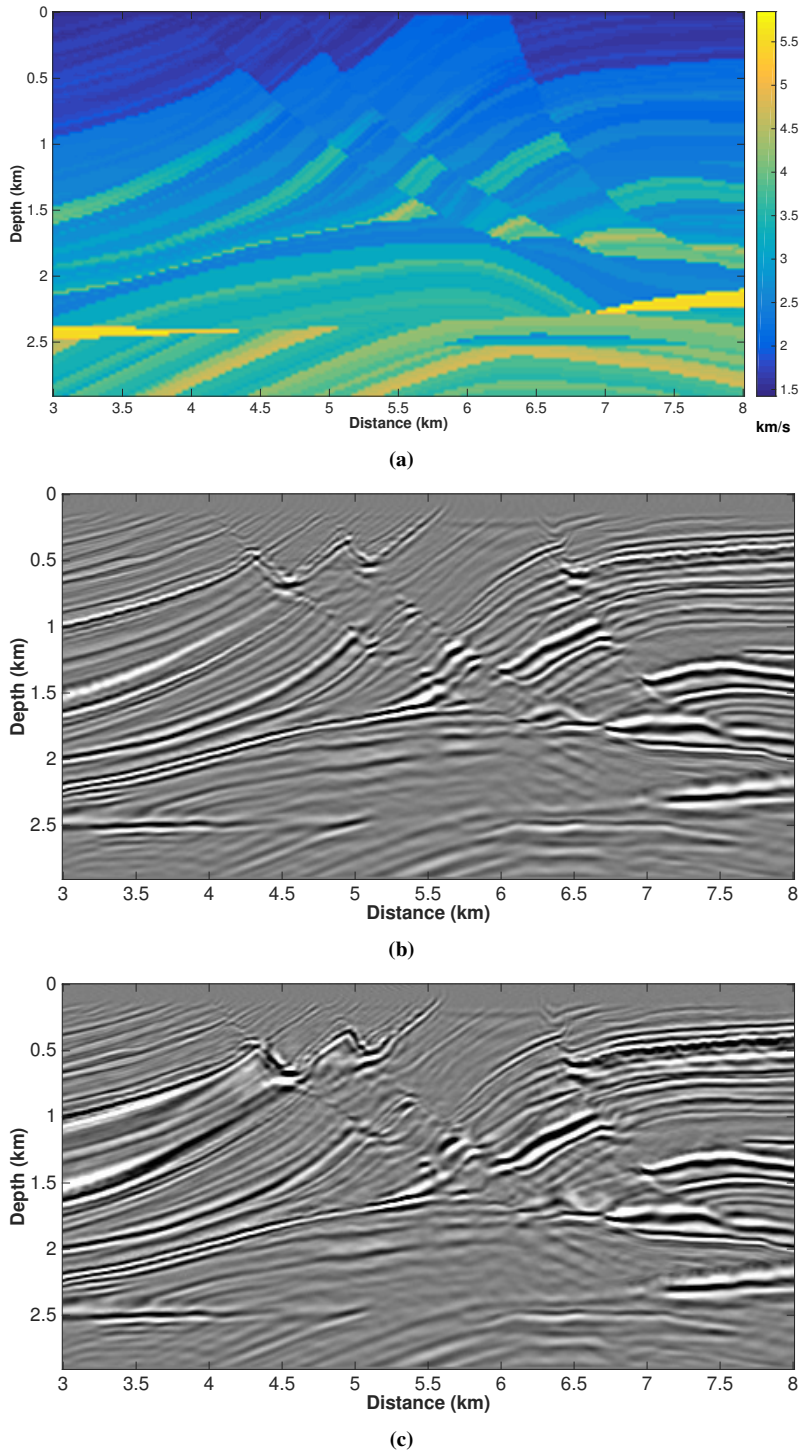

Figure 13: (a) Marmousi velocity model. Prestack depth migration of Marmousi data set using (b) complex wide-angle FFD produced by Amazonas et al. (2007) and (c) optimised complex wide-angle FFD. The latter image was computed with approximately the half of the time expended for the first one.

the complex Padé expansions. For this purpose, we determined, for each velocity ratio, the value of σ that made a one-percent error of the dispersion relation occur at the maximum possible dip angle. Using these

optimised σ functions, we noticed the need to reevaluate the branch-cut rotation angle α and the number of terms in the complex Padé expansion, because the algorithm behaves differently for better σ than for the theoretical expression or a heuristic function.

Our main result is that the best maximum dip angles of more than 65 degrees can be reached with a one-term Padé approximation with a small branch-cut rotation angle of 5 degrees. These angles are about the same as those reached with real-Padé FFD using the optimised σ but the advantage is that the complex algorithm presents an improved treatment of evanescent modes. Surprisingly, using two terms in the Padé expansion leads to higher maximum dip angles only for velocity ratios below 0.7. The use of three terms turns out not to be advisable as it increases computation cost without improvement in the maximum dip angle.

The optimal σ function for the one-term, 5°, approximation turned out to be a smooth curve that could be nicely adjusted with a 4th-order polynomial. First results of CPFFD migration with the optimised parameters applied to synthetic data from the Marmousi model showed similar quality to those obtained using the more expensive parametrisation from the literature. Future investigations will have to show whether independent optimisation of the parameters for the higher-order Padé terms can lead to further improvements.

ACKNOWLEDGMENTS

This work was kindly supported by the sponsors of the *Wave Inversion Technology (WIT) Consortium*. We acknowledge Petrobras and CGG as well as the Brazilian national research agencies CNPq, FAPESP, FINEP and CAPES. Marco Salcedo thanks CAPES for his fellowship. Henrique B. Santos is grateful to CGG-Brazil and Petrobras for his fellowships.

REFERENCES

Amazonas, D., Costa, J. C., Schleicher, J., and Pestana, R. (2007). Wide-angle FD and FFD migration using complex Padé approximations. *Geophysics*, 72(6):S215–S220.

Bamberger, A., Engquist, L. H., and Joly, P. (1988). Higher order paraxial wave equation approximations in heterogeneous media. *Journal of Applied Mathematics*, 48:129–154.

Biondi, B. (2002). Stable wide-angle Fourier finite-difference downward extrapolation of 3-D wavefields. *Geophysics*, 67(3):872–882.

Claerbout, J. F. (1985). Imaging the earth's interior. *Blackwell Scientific Publications, Inc*.

Gazdag, J. (1978). Wave equation migration with the phase-shift method. *Geophysics*, 43:1342–1351.

Gazdag, J. and Sguazzero, P. (1984). Migration of seismic data by phase-shift plus interpolation. *Geophysics*, 49:124–131.

Milinazzo, F. A., Zala, C. A., and Brooke, G. H. (1997). Rational square-root approximations for parabolic equation algorithms. *The Journal of the Acoustical Society of America*, 101(2):760–766.

Ristow, D. and Rühl, T. (1994). Fourier finite-difference migration. *Geophysics*, 59(12):1882–1893.

Stoffa, P. L., Fokkema, J. T., de Luna Freire, R. M., and Kessinger, W. P. (1990). Split-step Fourier migration. *Geophysics*, 55:410–421.

Versteeg, R. (1994). The Marmousi experience: Velocity model determination on a synthetic complex data set. *The Leading Edge*, 13(9):927–936.

Wapenaar, K., Thorbecke, J., van der Neut, J., Broggini, F., Slob, E., and Snieder, R. (2014). Marchenko imaging. *Geophysics*, 79(3):WA39–WA57.